Distinct microbial response to organic matter from nitrogen-starved and virus-infected phytoplankton

Shira Givati (1, 2), Eyal Rahav (2, 3, 4), Osnat Weissberg (1), Dikla Aharonovich (1), Noga Barak (1), Qinglu Zeng (5) and Daniel Sher (1)

(1) Department of Marine Biology, University of Haifa, Haifa, Israel

(2) Israel Oceanographic and Limnological Research, National Institute of Oceanography, Tel Shikmona, P.O. Box 8030, Haifa 31080, Israel

(3) Institute of Marine Science, University of California, Santa Cruz, CA, USA.

(4) Department of Earth and Environmental Science, Ben-Gurion University of the Negev, Beer Sheva, Israel.

(5) Department of Ocean Science, Hong Kong University of Science and Technology. Hong Kong SAR, China.

Abstract

When phytoplankton die they release dissolved organic matter (DOM) that feeds co-occurring heterotrophic bacteria. We show that death due to phage infection and nitrogen starvation result in different changes to the macromolecular structure of *Prochlorococcus*, a globally abundant cyanobacterium, and that the resulting DOM elicits different microbial responses. Viral infection led to increased RNA and DNA content in *Prochlorococcus* whereas nitrogen starvation led to a lower protein content. DOM released from phage-infected cells induced high secondary (bacterial) production, while DOM from starved cells increased dark (heterotrophic) primary production in natural microbial communities from the oligotrophic Eastern Mediterranean Sea. Through 16S and 18S amplicon sequencing, metagenomics, and laboratory experiments we identify

Alteromonadaceae and *Rhodobacteraceae* as heterotrophic taxa responding differently to the two DOM sources. We propose that distinct forms of phytoplankton mortality drive shifts in microbial community metabolism, including differential activity of pathways for heterotrophic carbon fixation, likely through anaplerotic reactions.

Introduction

Heterotrophic bacteria in the ocean rely on dissolved organic matter (DOM) released by phytoplankton, including cyanobacteria, as a primary resource for growth [1,2]. DOM is released by phytoplankton as they grow (e.g. through exudation or vesicle release, [3]), and as they die, with the specific cause of death potentially affecting the biochemical structure of the phytoplankton and the composition of the released DOM. For example, *Prochlorococcus*, which is the numerically most abundant phytoplankton cell in the oligotrophic oceans [4], contributes ~8.5% of the net global marine primary productivity estimated at ~4 Gt C y^{-1} [5]. As *Prochlorococcus* cells die, they release a diverse mixture of organic compounds, thereby altering the complex DOM pool in the water column [6–8]. *Prochlorococcus* die mostly through grazing, phage infection and "other" sources of mortality such as UV damage and, potentially, nutrient starvation, but the relative contribution of each cause of death is currently not well constrained. Estimates range between ~66-96% for grazing, 4-40% for phage infection and 1-27% for "other" sources of mortality including starvation [9–12]. Given that the pulse of organic carbon (C) released when *Prochlorococcus* cells die could account for more than 75% of the daily production at the surface of the oligotrophic ocean [13], understanding what affects the composition of this

43 photosynthetically fixed C and how it affects the surrounding microbial ecosystem could be of
44 significant biogeochemical and ecological importance.

45 Different types of mortality, such as starvation and phage infection, can alter the composition of
46 released DOM because each cause of death is associated with distinct changes in cellular
47 physiology, resource allocation and macromolecular structure. *Prochlorococcus* cells
48 experiencing nitrogen starvation in the lab have decreased levels of protein and RNA along with
49 elevated carbon content, potentially from storage carbohydrates or lipids [14,15]. Similar changes
50 are seen also in other phytoplankton [16,17]. In contrast, little is known about how virus or phage
51 infection affects the macromolecular structure of phytoplankton, but since phage infections results
52 in the production of protein- and nucleic-acid rich virions, these pools are expected to increase
53 [18]. Indeed, phage infection has been shown to change host metabolism and biochemical
54 composition (metabolite composition, [19–21]). As the cells die and lyse, the changes in
55 macromolecular structure are expected to result in concomitant changes in the released DOM
56 [22,23].

57 Once DOM is released from the dying cells, it fuels secondary bacterial production and growth
58 by surrounding heterotrophic bacteria [24]. During exponential growth in the lab, *Prochlorococcus*
59 releases a variety of organic compounds, including highly labile compounds - amino acids and
60 carboxylic acids such as pyruvate, acetate, and formate [6,25–29]. As the cells die and lyse, they
61 release also cell biomass, which is expected to be enriched in larger and more complex
62 macromolecules such as RNA, DNA, large protein complexes, lipids and other storage polymers.
63 *Prochlorococcus* viral lysate was found to contain more labile, bioavailable DOM (e.g., amino
64 acids, protein-like, and low-molecular-weight compounds), promoting greater bacterial growth
65 than *Prochlorococcus* exudate [22]. In addition, each of these different types of macromolecules

can fuel the growth of different heterotrophic bacteria [30–33]. Therefore, it is expected that changes in the biochemical structure of the cells due to different forms of mortality could impact the structure and function of surrounding heterotrophic communities. Indeed, previous studies have suggested that phytoplankton cell lysis due to viral infection (including in *Prochlorococcus*) enhances net productivity and organic matter recycling, significantly more than in ecosystems with low viral infection [22,34–37]. In the ocean, this process is known as the "viral shunt" ~~[38,39]~~, which plays a crucial role in oceanic biogeochemical cycles by influencing the microbial loop and facilitating the recycling of organic carbon within the marine environment ~~[34]~~.

Here, we directly compare how nitrogen starvation and phage infection affect cell quotas of protein, RNA and DNA in *Prochlorococcus* (Figure 1A). We chose to measure these major macromolecular pools as they are the main constituents of cell biomass, determining the elemental ratio of the cells [40,41]. These macromolecules are also emerging as important variables in phytoplankton models from the cellular to ocean scales [15,42]. We then amended surface seawater from the oligotrophic Eastern Mediterranean Sea (EMS) with DOM derived either from nitrogen-starved *Prochlorococcus* (hereafter referred to as treatment nSM) or viral lysate (treatment vSM) (Figure 1A). As expected, we observed increased secondary production due to vSM, but surprisingly we also observed increased dark carbon fixation (DCF) in response to nSM. To investigate the microbial taxa driving this response (i.e., fix CO_2 in response to nSM), we employed 16S and 18S amplicon sequencing, metagenomic analyses and targeted experiments using specific bacterial isolates. Ultimately, by dissecting the differential release of organic compounds under starvation and phage infection, we aim to gain a deeper understanding of *Prochlorococcus*'s role in marine carbon cycling and its complex interactions within ambient marine microbial ecosystem.

Results and discussion

Phage infection and nitrogen starvation differently affect Prochlorococcus macromolecular composition

We first compared how phage infection and nitrogen starvation influence the macromolecular composition of *Prochlorococcus* MED4 (Figure 1). Cultures were infected by myovirus P-HM2 during early to mid-logarithmic growth, with samples collected after 12 hours post infection (hpi, after one round of infection and lysis [19]), and after 36 hpi when most of the culture has been lysed (likely after several rounds of infections) (Figure 1B). The uninfected cultures were sampled at the same time points, as well as during mid-decline, following the onset of nitrogen starvation (day 14, Figure S1C [43]). Protein quotas per cell, and to lesser extent those of RNA and DNA, decreased in the N-starved *Prochlorococcus* (Figure 1C-E), consistent with prior observations [14,15]. In contrast, RNA and DNA quotas increased for the infected *Prochlorococcus,* and protein quotas remained unchanged (Figure 1C-E).

The increase in intracellular DNA is consistent with synthesis of phage genomic DNA, since P-HM2 has a double-stranded DNA genome [44], but the increase in cellular RNA is more perplexing. In most cells, ribosomes contain ~80-90% of the total RNA [45], and if this is true in this case it would suggest that the number of ribosomes remains similar or even increases, despite phage infection shutting down major aspects of cell physiology [46]. A previous study of P-HM2 infection in *Prochlorococcus* MED4 showed a decline in host transcripts related to translation and ribosomal proteins, with phage-derived mRNA levels exceed those of the host genes [47]. Some phages encode ribosomal proteins such as bS21 and bL12, which could potentially help stabilize the host ribosomes and/or increase their production [48,49], but no such proteins have been

111 described in P-HM2. It is possible that P-HM2 encodes other proteins or RNAs that stabilize the
112 ribosome. Alternatively, it is possible that most of the measured RNA is in fact phage RNA, and
113 in this case it is possible that ribosomes are in fact depleted, as observed in SAR11, where a
114 substantial fraction (7–15%) of infected cells were found to be 'ribosome-deprived zombie cells'
115 [50]. Even if this is true, phage P-HM2 is still able to tightly control the metabolism of its hosts,
116 including potentially protein translation rates, thus avoiding mispackaging of new virions with
117 host rather than viral DNA [47,51].

118 The DOM released following cell lysis due to phage infection ("viral spent media", vSM) and
119 nitrogen starvation ("nitrogen-starved spent media", nSM) also differed. Dissolved organic carbon
120 (DOC) was approximately 2 to 3 times higher in the spent media from nitrogen-starved
121 *Prochlorococcus* (nSM) compared to that from infected *Prochlorococcus* (vSM) (500–650 µmol
122 C L^{-1} versus 200–250 µmol C L^{-1}, respectively, Figure 1G). In contrast, dissolved organic nitrogen
123 (DON) concentrations were similar, leading to significantly (P-value<0.05, t-test) higher C:N ratio
124 (DOC:DON) in the nSM (Figure 1H, I). This is consistent with previous studies suggesting high
125 DOC release from nitrogen-starved *Prochlorococcus*, potentially due to "overflow metabolism"
126 as the cells continue to fix carbon without being able to form new biomass, thus releasing carbon-
127 rich molecules [7,8,26,52,53]. In contrast, dissolved DNA was measurable only in the vSM (Figure
128 1F), likely representing released phage particles. Indeed, the vSM contained infective phages
129 (Figure S2).

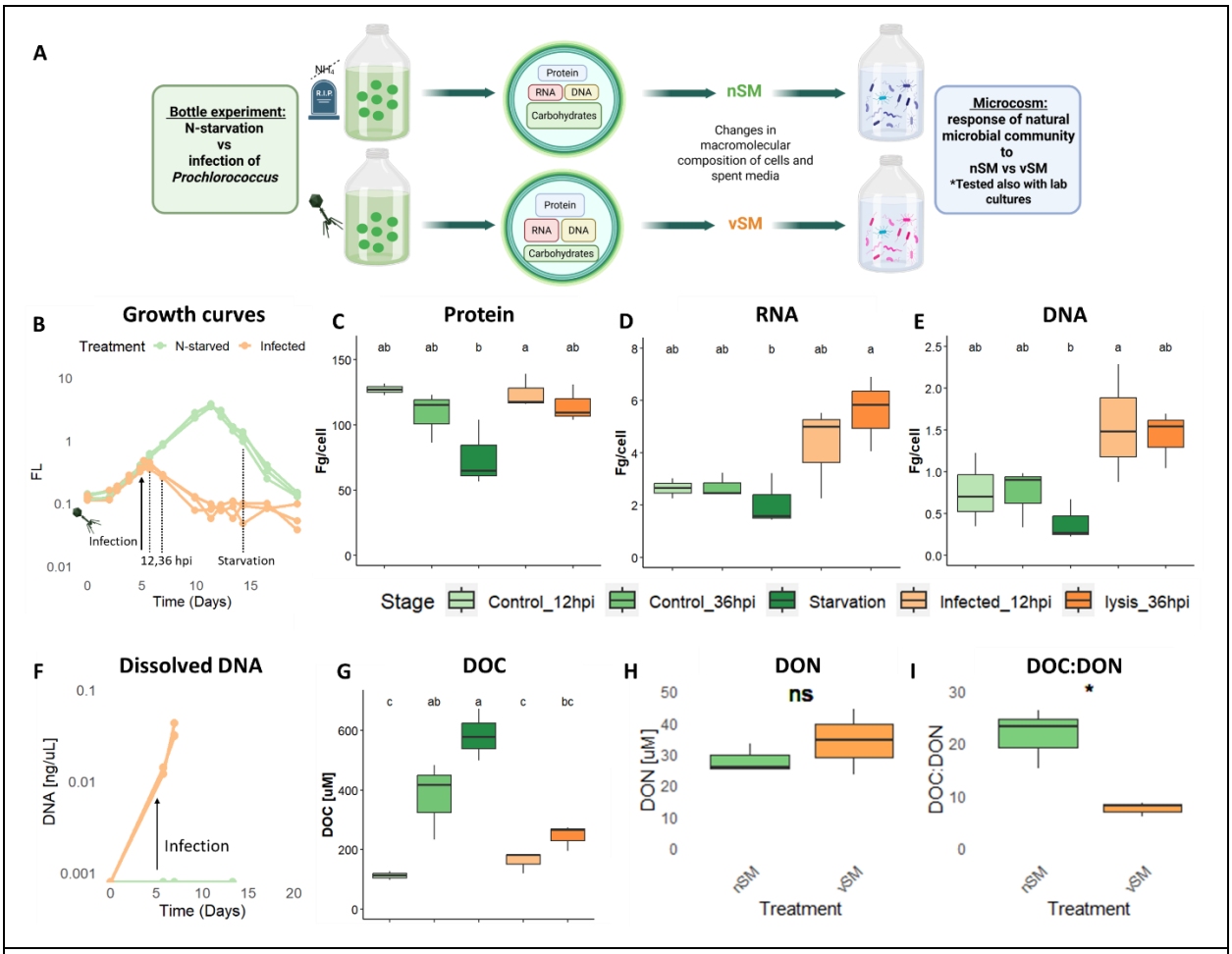

Figure 1. **Effect of nitrogen starvation and phage infection on the macromolecular composition of *Prochlorococcus* MED4**. (A) Illustration of the experimental set-up. (B) Growth curves of N-starved (green) and infected (orange) *Prochlorococcus* – fluorescence, a proxy for cells numbers. (C) Protein quotas in *Prochlorococcus* cells. (D) RNA quotas. (E) DNA quotas. (F) Dissolved DNA nSM (green) and vSM (orange). (G) Dissolved organic carbon (DOC) concentrations. (H) Dissolved organic nitrogen (DON) in nSM and vSM. (I) DOC:DON ratio in nSM and vSM. Box-Whisker plots show the interquartile range (25th–75th percentile) of the data set. The horizontal line within the box represents the median value (N=3). The different letters above the box plots (C, D, E, G) indicate statistically significant differences among the treatments (one-way ANOVA and post-hoc Tukey test, $p < 0.05$). Asterisks above the box plots (H, I) indicate statistically significant differences between treatments based on t-tests ($p < 0.05$). Abbreviations: hpi = hours post infection; nSM- spent media following nitrogen starvation; vSM - viral spent media.

130

131 *DOM from N-starved and infected Prochlorococcus has distinct effects on bacterial activity and*
132 *dark carbon fixation in natural microbial communities*

133 We next added nSM and vSM to natural microbial communities from the Eastern Mediterranean
134 Sea (EMS) in two separate experiments, one during autumn, when the water column was highly
135 stratified and oligotrophic (Figure S3A-C), and another during spring, when the water column was
136 mixed and nutrients concentrations were much higher (Figure S3D-F). The amendments contained
137 equal amounts of DOC (25 μM, a concentration used in previous studies [30,54]), as well as NH_4^+
138 and PO_4^{2-} to make sure the microbial communities were not nutrient-limited and could thus
139 respond to the potentially different compositions of organic carbon sources.

140 During both autumn and spring, the addition of vSM led to a significant (*P*-value<0.05, ANOVA)
141 increase in total cell counts compared to the control where only inorganic nutrients were added,
142 whereas the addition of nSM did not result in a significant change (Figure 2A, Figure S4A). Further
143 examination of the flow cytometry scattergrams indicated that the differences between the nSM
144 and vSM in both experiments were primarily due to a higher increase in the number of low nucleic
145 acid (LNA) cells in response to vSM (*P*-value<0.01, ANOVA, Figure S4C). LNA cells,
146 characterized by reduced fluorescence intensity, small cell size, and compact genomes, are highly
147 abundant in oligotrophic oceans, yet their precise identity remains uncertain [55]. In this study, the
148 LNA population exhibited a larger increase in the intensity of Sybr-green staining in the vSM (*P*-
149 value<0.001, ANOVA, Figure S4F, G). Assuming that the intensity of Sybr-green staining is
150 related to the nucleic acid content of the cells, this might suggest that LNA cells increased both in
151 abundance and activity [56], primarily in response to vSM. Bacterial production (BP), measured
152 as the incorporation of radioactive leucine, also increased significantly during spring in response
153 to the vSM than the nSM (*P*-value<0.001, ANOVA, Figure S5D, BP measurements during autumn

154 were unreliable). Taken together, these results, including increased total cell counts, higher
155 abundance and activity of LNA cells, and elevated bacterial production, suggest that viral lysate
156 elicits faster growth and more heterotrophic activity compared to nSM. This is consistent with
157 experiments performed in the South China Sea with the lysates of P-HM2 and two other phages
158 compared with spent media from exponentially-growing *Prochlorococcus* [22].

159 In addition to BP, we also measured dark carbon fixation (DCF), the incorporation of CO_2 into
160 biomass without light energy. DCF can be performed by chemoautotrophs, which use inorganic
161 electron donors such as CO_2 or H_2, or by heterotrophic bacteria which use organic matter as a
162 source of energy (see details below). Heterotrophic CO_2 fixation is increasingly recognized as a
163 significant and previously overlooked contributor to CO_2 assimilation in marine environments,
164 occurring not only in the deep, dark ocean but also in shallower waters [33,57–62]. Intriguingly,
165 we observed a significant increase in DCF in the nSM but not vSM during both autumn (*P*-
166 value<0.001, ANOVA, Figure 2B, C) and spring (*P*-value<0.01, ANOVA, Figure S5B, C)
167 experiments, reaching in our experimental incubations levels comparable to photosynthesis in the
168 oligotrophic Mediterranean and Red Seas (see Supplementary text 1).

169

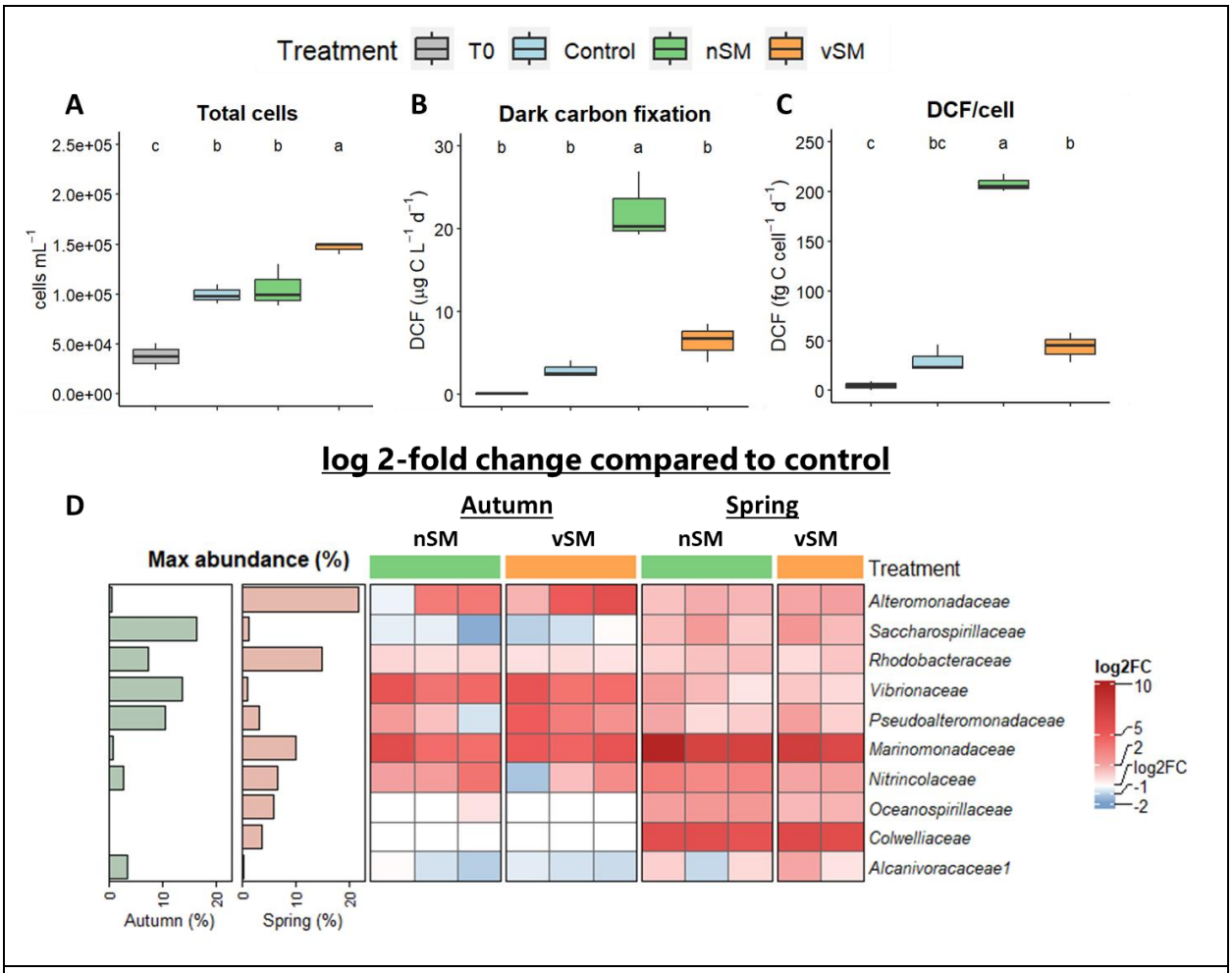

Figure 2. **Spent media from N-starved and infected *Prochlorococcus* differently affect natural microbial community activity and structure.** (A) Total cells count. (B) Dark inorganic carbon fixation (DCF). (C) Per-cell DCF. Box-Whisker plots show the interquartile range (25th–75th percentile) of the data set. The horizontal line within the box represents the median value (N=3). The different letters above the box plot indicate statistically significant differences among the treatments (one-way ANOVA and post-hoc Tukey test, $p < 0.05$). (D) Heatmap showing the $\log_2$ fold change in relative abundance of the top bacterial families enriched in the nSM and vSM compared to the control, based on 16S rRNA sequencing. Each column is an experimental replicate, and each row is a family for which at least one replicate showed a relative abundance above 1% and a fold change greater than 2 compared to the nutrient-only control. The bar-plots on the left of the heatmap show maximum relative abundance in nSM or vSM in the autumn (green) and spring (pink). For the full bar-plot of the community structure and more discussion please see Figure S6 and Supplementary text 2. Abbreviation: DCF – dark carbon fixation; nSM- spent media following nitrogen starvation; vSM - viral spent media.

170

171 *16S amplicon sequencing reveals no specific clades enriched in the nSM that could be associated*
172 *with DCF*

173 We expected the differences in the functional response to nSM and vSM to be mirrored by
174 differences in the community structure, as assessed by amplicon sequencing of the 16S rRNA
175 (which is affected by both relative organism abundance and activity, i.e., number of ribosomes).
176 Specifically, we expected to identify organisms (represented by Amplicon Sequence Variants,
177 ASVs) which exhibit a higher increase in relative abundance in response to nSM than to vSM
178 compared to the no-DOM control. Such ASVs would be good candidate organisms responsible for
179 the increased DCF. However, while the nSM and vSM differed from the nutrient-only controls in
180 both autumn and spring experiments (Figure S6), no ASVs were specifically enriched in the nSM
181 (Figure 2D). Several bacterial families increased in relative abundance in both treatments
182 compared to the controls, including (during autumn) *Vibrionaceae*, *Pseudoalteromonadaceae* and
183 *Rhodobacteraceae* (Figure 2D, Figure S7). During spring, *Alteromonadaceae* rather than
184 *Pseudoalteromonadaceae* increased significantly in both treatments (Figure 2D). These results are
185 in agreement with previous experiments where spent media from *Prochlorococcus* was added to
186 natural communities [22,54,63].

187 During the Autumn experiment we sequenced also 16S rDNA amplicons (Figure S8), which
188 reflects relative abundance and not activity. *Pseudoalteromonadaceae* and *Vibrionaceae* increased
189 significantly in relative abundance in both rDNA and rRNA amplicons, suggesting rapid growth
190 in response to nSM and vSM. In contrast, the relative abundance of *Rhodobacteraceae* increased
191 only in the rRNA and not the rDNA, suggesting increased activity without necessarily a
192 concomitant increase in cell numbers. The specific *Vibrionaceae* and *Rhodobacteraceae* ASVs
193 responding during autumn and spring were not identical, suggesting temporal differences in the

194 fine-scale community structure or function between the two seasons (Figure S6). Analysis of 18S
195 rRNA sequencing from the autumn experiment revealed no significant changes in eukaryotic
196 community structure (Figure S9).

197 *Identifying clades with the capacity for DCF using metagenomics*

198 Since the 16S and 18S amplicon sequencing was not able to highlight microbial clades responsible
199 for the increased DCF, we next searched for relevant pathways (and, subsequently, individual
200 genes) in metagenomes from the nSM, vSM and control incubations. Broadly speaking,
201 *autotrophic* CO_2 fixation is mediated by pathways such as the reverse tricarboxylic acid (rTCA)
202 cycle or the Wood-Ljungdahl pathway [64]. In contrast, the primary process in *heterotrophic* CO_2
203 fixation is anaplerosis, the replenishment of tricarboxylic acid (TCA) cycle intermediates such as
204 oxaloacetate and malate (see below). Autotrophic CO_2 fixation pathways in prokaryotes (KEGG
205 pathway ko00720) were enriched in both the nSM and vSM compared to no-DOM controls, but
206 this was not statistically significant, and no clear difference was observed between the nSM and
207 vSM (Figure S10). This suggests that chemoautotrophy is not the main process responsible for the
208 observed DCF. Heterotrophic CO_2 fixation, which is composed of various individual genes (see
209 below), lacks a dedicated KEGG pathway, and therefore could not be assessed at the pathway
210 level. However, the nSM metagenome was enriched in pathways related to carbohydrate utilization
211 (e.g., the tricarboxylic acid (TCA) cycle and pyruvate metabolism), lipid metabolism (fatty acid
212 metabolism) and amino acids synthesis (e.g., valine, leucine, and isoleucine biosynthesis) (Figure
213 3). We interpret these results as evidence that C-rich molecules such as carbohydrates and lipids
214 were more abundant in the nSM compared with the vSM, consistent with the higher DOC:DON
215 ratio.

216 If indeed carbon-rich molecules are major components of the nSM, organisms utilizing them as
217 resources would likely need to produce their own nitrogen-rich building blocks such as amino
218 acids and nucleotides from TCA cycle intermediates, rather than taking them up from the
219 environment. In this case, the cell needs to compensate for flux diverted from the TCA cycle into
220 biosynthesis by using one or more of six specific anaplerotic reactions, four of which also include
221 a CO_2 fixation step (Figure 4A, [60]). Genes encoding the CO_2 fixing enzymes
222 phosphoenolpyruvate (PEP) carboxylase (PEPC), PEP carboxykinase (PEPCK) and malate
223 dehydrogenase (MDH) were relatively abundant in the metagenomes, whereas pyruvate
224 carboxylase (PC) was less common (Figure 4B). Overall, there was no significant difference in the
225 abundance of these genes between the nSM, vSM and controls (Figure 4B), yet in each treatment
226 the sequences of these genes primarily originated from different bacterial orders (Figure 4C). For
227 example, genes encoding PEPCK and MD from *Vibrionales* and *Rhodobacterales*, respectively,
228 were enriched in the nSM (~1.5-3.5 and ~2-4.5-fold change compared to vSM), suggesting these
229 clades might be involved in the observed DCF. In contrast, PEPC, PC and MD from
230 *Pelagibacterales* were enriched in the vSM (~1.4-2.8-fold change), as were PEPC from
231 *Pseudoalteromonadales* (~4-fold change), positioning these clades as less likely candidates for the
232 observed DCF. Similar results were observed also for genes encoding enzymes in the glyoxylate
233 shunt (malate synthase and isocitrate lyase), an anaplerotic process that does not include a CO_2
234 fixation step (Figure 4A). Genes encoding other heterotrophic CO_2 fixing enzymes, such as those
235 involved in leucin utilization or biotin production, were less common in the metagenomes (Figure
236 4B).

237 Analysis of metagenome-assembled genomes (MAGs) provided further support for hypothesis that
238 heterotrophic, rather than autotrophic, processes were involved in the DCF, as pathways encoding

239 the former were more commonly found and more complete within MAGs (Figure S11).
240 Anaplerotic genes were present at varying levels of completeness across all MAGs, with
241 *Rhodobacteraceae* MAG MED-G52 possessing all of the 4 CO_2-fixing genes (Figure 5). However,
242 the MAGs also further highlighted that there are other clades (primarily alpha and gamma
243 proteobacteria and flavobacteria) that have the genetic potential to perform DCF.

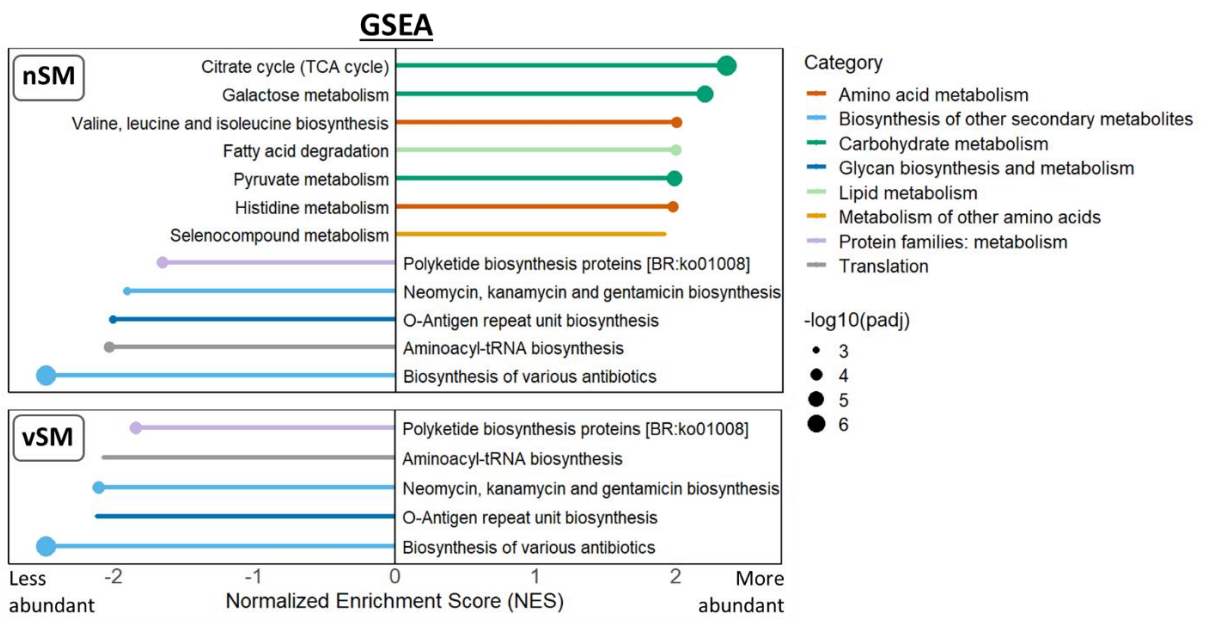

Figure 3. **Gene set enrichment analysis (GSEA) of differentially expressed genes in nSM and vSM**. Only statistically significant pathways (adjusted *p*-value < 0.05) are shown. The size of the bars represents the normalized enrichment score (NES). The size of the points represents the adjusted *p*-value. For expanded GSEA results see Figure S10.

244

245

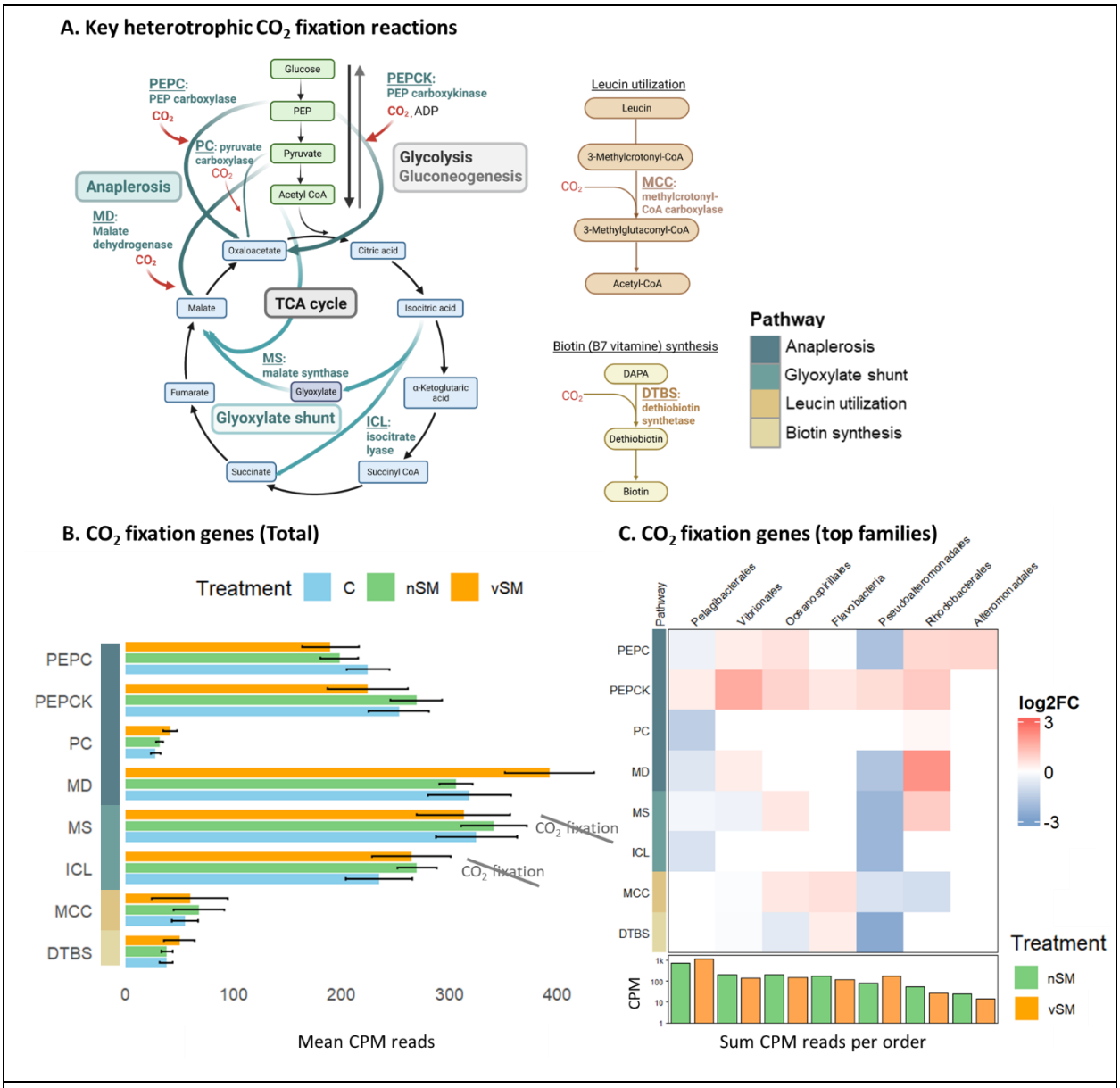

Figure 4. Metagenome analysis for CO_2 fixation pathways. (A) Diagram illustrating key heterotrophic CO_2 fixation reactions, along with the TCA, glyoxylate shunt and gluconeogenesis. DAPA: 7,8-diaminononanoate. Scheme was modified from Amano et al. [58]. (B) Total normalized reads (CPM)) for key enzymes associated with heterotrophic CO_2 fixation. (C) Heatmap for average (N=3) fold change of nSM relatives to vSM reads for major heterotrophic taxa, which exhibited the highest relative abundance of discussing genes (based on CPM reads, Figure S12). Bottom bar plots showing sum CPM reads of all genes for each bacterial family in nSM (green) and vSM (orange). Abbreviations: PEPC - phosphoenolpyruvate (PEP) carboxylase; PEPCK - PEP carboxykinase; PC – pyruvate carboxylase; MDH - malate dehydrogenase; MS – malate synthase; ICL – isocitrate lyase; MCC - methylcrotonyl-

CoA carboxylase; DTBS - dethiobiotin synthetase. Although ICL and MS have anaplerotic role, they are not involved in CO_2 fixation – for more details see Supplementary text 3.

246

247 *Cultured Rhodobacterales and Alteromonadales strains perform higher DCF in response to nSM*
248 *compared to vSM*

249 The metagenomic analysis highlights *Rhodobacterales* and *Alteromonadaceae* (as well as
250 *Oceanospirillales* and *Vibrionales*) as orders potentially involved in the higher DCF in nSM
251 treatment, and *Pseudoalteromonadales* and *Pelagibacterales* as relatively abundant clades less
252 likely to do so (Figure 4C). To begin testing these hypotheses, six laboratory cultures, representing
253 the major orders found in our metagenome analyses, were starved for carbon to simulate
254 oligotrophic conditions followed by the addition of nSM and vSM (Supplementary text 4). Two
255 of the strains, *Alteromonas mediterranea* strain DE (*Alteromonadales*) and *Marinovum* strain
256 HOT5_F3 (*Rhodobacterales*), exhibited elevated per-cell DCF in the nSM (Figure 5), reminiscent
257 of the observations in the field experiments (Figure 4C). None of the strain exhibited significantly
258 higher DCF in response to vSM. Bacterial production also increased more in *Alteromonas* in
259 response to nSM compared to vSM, and thus the DCF could, in principle, represent stronger overall
260 growth. In contrast, only DCF increased in *Marinovum*, suggesting a specific metabolic response
261 that is not coupled with growth, at least not in the time-frame of the experiment. This is similar to
262 the response of the *Rhodobacterales* in the two experiments with natural microbial populations
263 (Figure 3C).

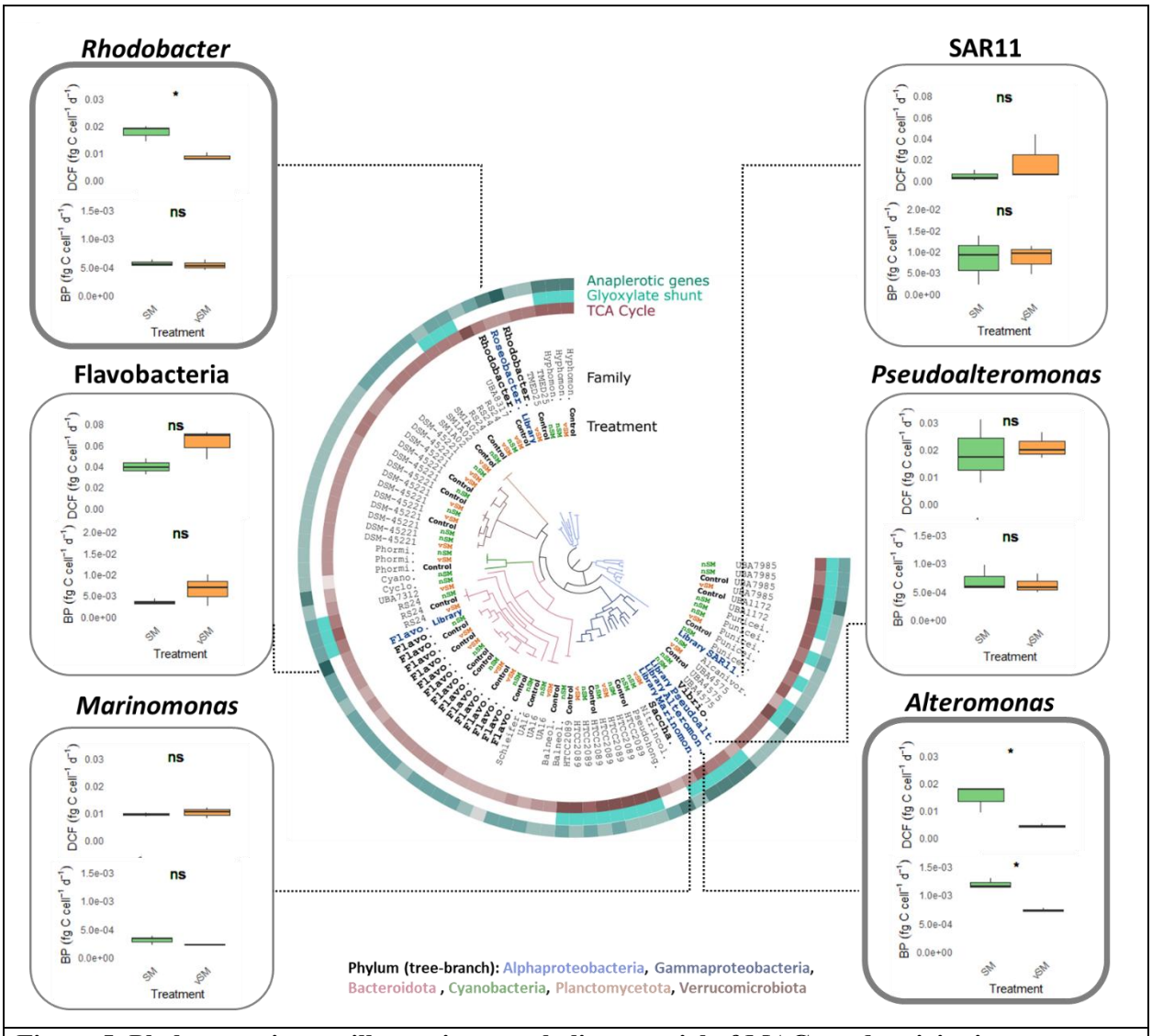

Figure 5. **Phylogenomic tree illustrating metabolic potential of MAGs and activity in response to vSM and nSM of representative laboratory taxa**. The outer rings indicate the presence of genes related to the TCA cycle, glyoxylate shunt, and anaplerotic pathways. Taxa are further annotated by bacterial family (inner ring) and treatment condition (control: black, nSM: green, vSM: orange). Bacterial taxa discussed in Figure 4C are highlighted in bold, and genomes derived from laboratory cultures are shown in blue. Boxplots adjacent to the tree illustrate per-cell dark inorganic carbon fixation (DCF) and bacterial production (BP) rates (in fg C cell^{-1} d^{-1}) for selected laboratory strains that belong to the orders displayed in Figure 4C. An asterisk (*) denotes statistically significant results (p-value < 0.05), determined by a paired t-test with Bonferroni correction. Note the distinct Y-axis scales for *Flavobacteria* and SAR11 compared to other strains, likely attributable to their lower cell counts as measured by flow cytometry (Figure S13A).

Abbreviations for the family level: Alcanivor. – *Alcanivoracaceae*; Alteromon. – *Alteromonadaceae*; Balneol. – *Balneolaceae*; Cyano. – *Cyanobiaceae*; Cyclo. – *Cyclobacteriaceae*; Flavo. – *Flavobacteriaceae*; Hyphomon. – *Hyphomonadaceae*; Marinomon. – *Marinomonadaceae*; Nitrincol. – *Nitrincolaceae*; Phormi. – *Phormidesmiaceae*; Pseudoalt. – *Pseudoalteromonadaceae*; Pseudohong. – *Pseudohongiellaceae*; Punicei. – *Puniceispirillaceae*; Rhodobacter. – *Rhodobacteraceae*; Saccha. – *Saccharospirillaceae*; Schleif. – *Schleiferiaceae*; Vibrio. – *Vibrionaceae*.

Abbreviations for the library strains (in blue): Alteromon. – *Alteromonas mediterranea* DE; Flavo. – *Formosa agariphila* KMM; Marinomon. – *Marinomonas mediterranea* MMB1; Pseudoalt. – *Pseudoalteromonas haloplanktis* TAC; Roseobacter. – *Roseobacteraceae Marinovum* HOT5_F3 (order of *Rhodobacterales*); SAR11 - Candidatus pelagibacteraceae St. HTCC1062 (refer to Table S1 for full details).

Summary and Conclusions

There are many ways microbial cells can die in the oceans. In laboratory cultures, whether *Prochlorococcus* MED4 dies due to phage infection or nitrogen starvation affects its biochemical structure, and the composition of DOM released upon death. In turn, these changes can have cascading effects on the microbes in the surrounding seawater, including shifts in bacterial community activity, metabolism, structure and function. DOM released through viral lysis increased overall heterotrophic community production, in agreement with a recent study [65], but we show for the first time that DOM from nutrient-starved cells increases heterotrophic CO_2 fixation (Figure 6).

In theory, phytoplankton biomass provides a "balanced meal" of building blocks (amino acids, nucleotides) and energy-rich molecules (carbohydrates, lipids) for heterotrophic bacteria [8,54]. However, the biochemical composition of the “meal” can change in response to different forms of death. Under nutrient starvation, phytoplankton like *Prochlorococcus* may shift towards producing and releasing excess carbon-rich metabolites, such as carbohydrates, through a process known as "overflow metabolism" [6,53,66]. Previous studies have shown that a significant portion of the

280 carbohydrates released by *Prochlorococcus* are carboxylic acids such as pyruvate, glycolate,
281 acetate and citrate (~4-20%, [6,25–28,53,66]). These carboxylic acids either feed directly into the
282 TCA cycle or are components of the cycle itself. We propose that such molecules (or their
283 polymeric forms, e.g. lipids) comprise a larger part of the DOM released during starvation
284 compared with phage lysis. We also propose that heterotrophic bacteria will need to employ
285 anaplerotic reactions to enable them to utilize these carbon-rich molecules as resources for both
286 energy and as backbones for biosynthesis of proteins and nucleic acids, e.g. using inorganic
287 nitrogen sources. In support of this hypothesis, the DOC:DON ratio of the nSM was higher than
288 that of the vSM, and pathways such as the TCA cycle, pyruvate metabolism, and fatty acid
289 degradation were enriched in the community responding to the nSM (Figure 6).

290 Additionally, two of the clades shown to respond to nSM by growth and/or DCF, *Alteromonadales*
291 and *Rhodobacterales,* respond in the lab and in the field to additions of organic acids,
292 monosaccharides and disaccharides [30,67–70]. Amano et al. [58] also demonstrated that
293 *Alteromonas* DE exhibits higher DCF rates on glucose compared to alanine, further supporting our
294 hypothesis that carbon-rich DOM contributes to elevated DCF. Both of these clades are often
295 associated with phytoplankton blooms and exudates, particularly those of cyanobacteria [71,72].
296 Taken together, these results, as well as previous studies, suggest an important role for these
297 bacterial clades in anaplerotic CO_2 fixation in the oceans [58,70,73,74].

298 In contrast to nitrogen starvation, cyanophage infection has been shown to increase the release of
299 nitrogen-rich compounds like amino acids [1,22]. This suggests that DOM released by phage
300 infection, and, potentially, phage themselves, are a source of bioavailable nitrogen, and potentially
301 also other limiting nutrients such as phosphorus [75–77]. We propose that the larger increase in
302 *Pseudoalteromonadaceae* abundance observed following vSM exposure in the autumn experiment

303 was due to vSM's nitrogen-rich composition, since cultured representatives of this clade
304 demonstrated preferences for peptides in laboratory cultures and field incubations [30,67]. It is
305 currently unclear whether the heterotrophic bacteria utilize nitrogen-rich lysate molecules such as
306 cellular proteins or nucleic acids, or whether they take up and metabolize the phage themselves.

307 Our findings align with a global ocean metatranscriptomic study highlighted the ubiquitous
308 expression of anaplerotic and glyoxylate shunt genes, often exceeding those involved in
309 chemoautotrophy [58]. If, indeed, a fraction of this heterotrophic CO_2 fixation is due to the
310 presence of organic matter released due to nutrient starvation, this could have important
311 consequences for understanding the cycling of dissolved organic carbon pools in the ocean. The
312 relative contribution of different forms of death - grazing, phage infection and nutrient starvation
313 – to the overall mortality of *Prochlorococcus* is still not well known [9–12]. However, it is
314 intriguing that in the oligotrophic Gulf of Eilat, higher DCF rates occurred during the oligotrophic
315 summer (~12% vs. ~7.5% in winter), supporting the link between nutrient scarcity and increased
316 DCF [61]. It is also important to note that the increase in the released DOC:DON ratio does not
317 necessarily require cell death, but can also occur as a result of overflow metabolism where fixed
318 carbon is released when there is not enough N/P/Fe to fuel cell growth [78]. These processes
319 (overflow metabolism and/or nutrient starvation) could be important processes responsible for
320 increased DOC in the subtropical gyres [79]. Taken together, these results provide additional
321 motivation to determine to what extent there exists a close coupling between specific forms of
322 mortality, the release of DOM and its subsequent metabolism, the temporal succession of microbes
323 in the sea (e.g. the succession of heterotrophic bacteria during phytoplankton blooms) and
324 biogeochemical cycles.

325

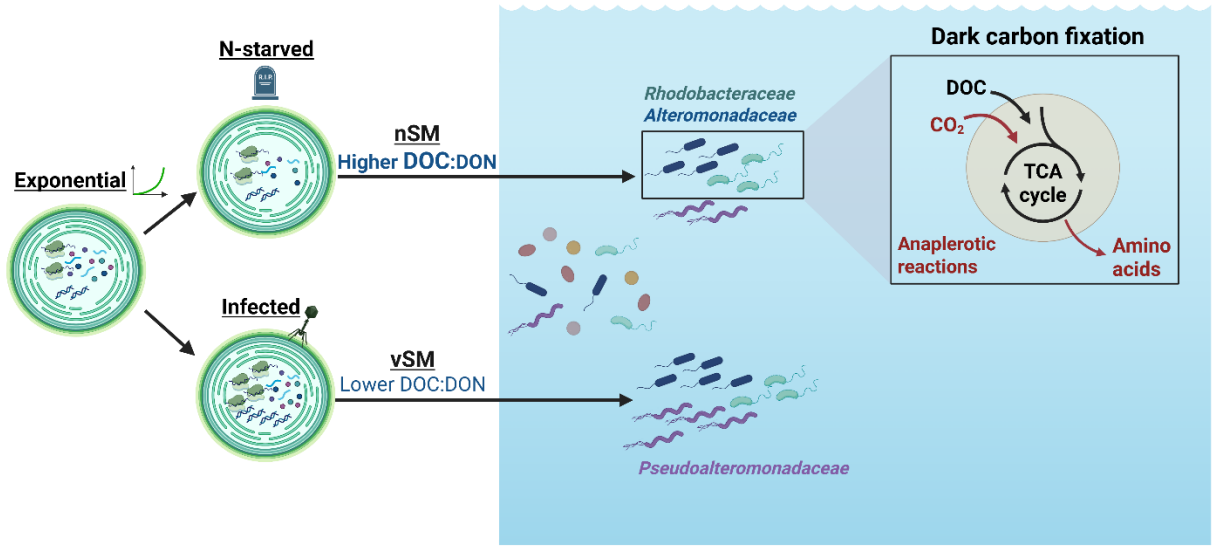

Figure 6. **Summary illustration of experimental observations and suggested mechanism**. Phage infection resulted in increased RNA and DNA quotas, whereas nitrogen-starved cells showed decreased protein quotas compared to logarithmic growth. Starved cells released more DOC concentration, while infected cells released more virions, found as dissolved DNA in the viral spent media (vSM). Addition of vSM resulted in increased total cells count and bacterial productivity. Addition of nSM increased dark inorganic carbon fixation (DCF) in both microcosm experiments and cultures of *Rhodobacterales and Alteromonadales*, which were also observed in the 16S rRNA analysis. Metagenomic analysis revealed an enrichment of pathways in the nSM treatments, including the TCA cycle, pyruvate metabolism, and phospholipid degradation.

Materials and Methods

***Prochlorococcus* bottle experiment: experimental setup and samples collection.** Triplicate bottles containing 750 mL of *Prochlorococcus* MED4 were grown in low-nitrogen media (lowN, [43]): Mediterranean sweater (MSW) supplemented with 200µM NH_4, 50µM PO_4 and 10,000X trace metals [80]. After 5 days, half of the bottles were inoculated with cyanophage P-HM2 at MOI of 2:1 (viable phage particles were counted using plaque assay, see Supplementary text 5 for further details). P-HM2 is a T4-like myovirus with a latent period of approximately 5 hours

334 [22,81]. Cells were infected on day 5, during early-to-mid logarithmic growth. Sampling occurred
335 at three timepoints: T1 (~12 hpi, following at least one round of infection), T2 (~36 hpi, following
336 several infection cycles), and T3 (uninfected samples only) captured the mid-decline stage for the
337 N-starved culture (Figure 1B) (See Supplementary text 6 for more details on specific samples).

338 **Cruise and microcosm experimental set-up.** Spent media from nitrogen-starved (nSM) and
339 viral-infected (vSM) *Prochlorococcus* was introduced into surface seawater collected from the
340 EMS. This experiment was conducted twice: once in autumn (November 7, 2022) and once in
341 spring (March 28, 2024 during an IOLR transect cruise H51). Seawater for both experiments were
342 collected at station H05 (32.99°N, 34.50°E), an open ocean site, from a depth of 25m. The
343 experiment included 3 treatments: (1) "nSM", amended with spent media from N-starved cells (T3
344 in the bottle experiment), (2) "vSM", amended with lysate from infected cells (T2 in the bottle
345 experiment) and a control amended only with inorganic N and P. Final DOC, NH_4 and PO_4
346 concentration was set to 25 µM, 15 µM and 10 µM, respectively - levels of N and P corresponding
347 to the highest concentrations measured in the *Prochlorococcus*-derived DOM from either
348 experimental replicate. Triplicate bottles of 4L (autumn) and 400mL (spring) from each treatment
349 were incubated in dark for 24 hours.

350 **Measurements of bulk protein, RNA and DNA.** Samples for protein, RNA and DNA were
351 filtered on 0.7 µm GF/F filters and stored at -80°C until analysis. Proteins were extracted by
352 incubating the samples with lysis buffer at 37˚C for 30 minutes, followed by 10 min of sonication
353 in a water bath (Ultrasonic Cleaner AC-120H), and quantified using the bicinchoninic acid (BCA)
354 assay [82]. RNA was isolated from the filter using Trizol extraction [83], and DNA using Phenol-
355 Chloroform [84]. The concentration of both RNA and DNA was determined with the Qubit™
356 RNA HS Assay Kit and Qubit™ dsDNA HS Assay Kit, respectively.

357 **Measurements of NH_4, PO_4, DOC and DON in nSM and vSM.** Samples for NH_4 and PO_4 were
358 filtered through 0.2 µm polycarbonate filters and stored at -20°C until analysis. Prior to
359 measurements, samples were diluted 4-fold in DDW to reduce the salt level. NH_4 was measured
360 using an HI 96715 meter (Hanna instrument), and PO_4 using Phosphate Colorimetric Assay Kit
361 (Catalog Number MAK030). Samples for dissolved organic carbon (DOC) and total nitrogen (TN)
362 were filtered through 0.2 µm polycarbonate filters, and are further elaborated on Supplementary
363 text 7.

364 **Bacterial productivity and Dark carbon fixation.** Bacterial productivity (BP) was estimated
365 using the ^{3}H-leucine incorporation method [85] as detailed by Reich et al. [86]. Dark inorganic
366 carbon fixation (DCF) was measured using the ^{14}C incorporation method [87], with few
367 modifications [88], as described in details by Reich et al. [86].

368 **16S RNA and DNA extraction, DNA digestion, and cDNA synthesis.** The bacterial community
369 structure and activity were assessed through 16S and 18S rRNA and rDNA sequencing. For each
370 incubation bottle, 1–2 L of seawater was filtered onto 0.2 µm filters, preserved in lysis buffer, and
371 stored at −80°C until extraction. RNA and DNA were extracted using the NucleoSpin RNA Stool
372 and the PureLink™ Genomic DNA Mini Kit, respectively, according to the manufacturer's
373 instructions. RNA extraction included DNase treatment, followed by reverse transcription into
374 cDNA using the iScript cDNA Synthesis Kit.

375 **16S and 18S rRNA and rDNA sequencing.** 16S rRNA and rDNA sequencing was conducted
376 using primers 515F and 926R [89], targeting ~400 bp products. For 18S rRNA, primers
377 Euk_1391F and EukBR were used, targeting ~200 bp products. Sequencing protocols are
378 described in detail in Givati et al. [30]. Briefly, amplicons were generated using a two-stage PCR
379 protocol, and libraries were sequenced on an Illumina MiSeq platform (V3 chemistry, 2 × 300 bp

380 reads) with a 15% phiX spike-in. Library preparation and sequencing were performed at the
381 Genomics and Microbiome Core Facility, Rush University, IL, USA.

382 **16S rRNA and rDNA sequence analysis.** All sequences of both autumn and spring experiments
383 were analyzed together using the Dada2 pipeline [90] and the software packages R [91] and
384 Rstudio [92], as detailed in Givati et al. [30]. Forward and backward primers were trimmed, and
385 forward and backward reads were truncated after quality inspections to 230 and 200 bases,
386 respectively. After sequences merging, a consensus length of only between 353 and 366 bases was
387 accepted, discarding ~30% of sequences in the process. Finally, amplicon sequence variants
388 (ASVs) that have less than 100 in total (all samples) were removed, remaining with a total of ~720
389 ASVs. Silva database version 138 [93] was used for taxonomic assignment. All chloroplasts,
390 mitochondria, archaea, eukaryotes, and ASVs without any taxonomic affiliation were discarded
391 from downstream analyses. Full ASVs and taxonomy list of 16S rRNA and rDNA can be found in
392 Supplementary files 1 and 2. For details on 18S rRNA sequence analysis see Supplementary text
393 8.

394 **Metagenomics sequencing.** Shotgun metagenomic libraries were prepared using the Illumina
395 Nextera XT DNA Library Preparation Kit. A total of 9 samples were processed for dsDNA shotgun
396 library preparation. Sequencing was carried out on an Illumina NovaSeq X platform using a 2 ×
397 150 bp paired-end protocol. Approximately 900 million clusters were generated per lane on a 25B
398 flow cell.

399 **Metagenomics and MAGs construction.** Raw metagenomic reads were first assessed for quality
400 using FastQC [94], followed by quality filtering and trimming using the algorithm bbduk [95]. For
401 *De-novo* assembly, trimmed metagenomes were assembled using Megahit [96]. For each
402 biological treatment (Control/SM/vSM), we first pooled the replicate libraries and then performed

403 a combined assembly. Gene calls on each of the assembly files were made using [97]. All the gene-
404 level KEGG Ortholog (KO) functional annotation was performed using KOFamScan [98]. Gene-
405 and contig-level taxonomic classifications for each assembly were performed using CAT [99].
406 Trimmed short reads for each sample were mapped to the corresponding assemblies
407 (contigs/genes) and coverage information was generated using bowtie2 [100]. All gene- and
408 taxonomy-level CPM read counts are provided in Supplementary files 4 and 5 (combined) and in
409 Supplementary files 6 to 8 (separated by treatment). MAGs were reconstructed by binning
410 assembled contigs per condition (see Supplementary text 9 for more details).

411 **Differential Gene Set Enrichment Analysis (GSEA).** Differential Gene Set Enrichment Analysis
412 (GSEA) was performed using the fgsea R package [101]. Gene sets were defined based on the
413 KEGG pathway database, utilizing a table containing KO IDs, their corresponding functions, and
414 pathway assignments. Analysis was restricted to KO IDs identified in the metagenome and
415 metabolic pathways containing 10 to 500 KOs. GSEA was conducted with 10,000 permutations,
416 using fold-change values as the ranking metric. Gene sets with an adjusted p-value < 0.05 were
417 considered statistically significant.

418 **Statistics.** Data pre-processing and statistical analyses were performed using the R statistical
419 programming language [91,92] and on Linux ubunto20. One-way analysis of variance (ANOVA)
420 and post hoc Tukey test was performed to compare the treatments in lab and microcosms
421 experiments (Figure 2 and Figure 3) using multcompView [102] and dplyr [103] packages. Paired
422 t-test with Bonferroni correction was used to compare the means between treatments for each
423 bacteria (Figure 6) using the packages tidyverse v1.3.0 [104], rstatix [105], and ggpubr [106].
424 Microbial community differences between treatments in the NMDS plots were statistically
425 assessed by PERMANOVA on Bray-Curtis dissimilarity matrices, with 999 permutations to

426 determine significance using vegan package [107]. Plots were originated using the ggplot2
427 package [108].

428 **Data availability.** All forward and backward sequence reads were uploaded to NCBI under
429 umbrella project accession number PRJNA1291108: PRJNA1287306 (16S rRNA),
430 PRJNA1287330 (16S rDNA), PRJNA1291108 (18S rRNA) and PRJNA1302148
431 (metagenomics).

432 **Acknowledgements:** We thank Ximena Dubinsky for help with the BP measurements, Solvig
433 Pinnow and Hans-Peter Grossart for the DON measurements, Eyal Giesler and Edo Bar Zeev for
434 the DOC measurements, Anat Tsemel and Mike Krom for the inorganic nutrient measurements.
435 We also thank Abdiel Lázaro García and Laura Steindler for the SAR11 cultures, and Ankur
436 Naqib, Adit Chaudhary and Stefan Green from the Rush Research Bioinformatics Core for the
437 metagenomic analysis pipeline. This study was supported by the Israel Science Foundation (grant
438 number 1786/20 to DS) and by the National Science Foundation - United States-Israel Binational
439 Science Foundation (NSFOCE-BSF 1635070 and NSF-BSF 2246707 to DS).

440

441 ## References

442 1. Cai L, Li H, Deng J *et al.* Biological interactions with Prochlorococcus: implications for the marine
443 carbon cycle. *Trends Microbiol* 2024;**32**:280–91.

444 2. Biller SJ, Lundeen RA, Hmelo LR *et al.* Prochlorococcus extracellular vesicles: molecular composition
445 and adsorption to diverse microbes. *Environ Microbiol* 2022;**24**:420–35.

446 3. Biller SJ, Schubotz F, Roggensack SE *et al.* Bacterial Vesicles in Marine Ecosystems. *Science (80-)*
447 2014;**343**:183–6.

448 4. Biller SJ, Berube PM, Lindell D *et al.* Prochlorococcus: the structure and function of collective
449 diversity. *Nat Rev Microbiol* 2015;**13**:13–27.

450 5. Flombaum P, Gallegos JL, Gordillo RA *et al.* Present and future global distributions of the marine
451 Cyanobacteria Prochlorococcus and Synechococcus. *Proc Natl Acad Sci* 2013;**110**:9824–9.

452 6. Bertilsson S, Berglund O, Pullin MJ *et al.* Release of dissolved organic matter by Prochlorococcus. *Vie*
453 *Milieu/Life Environ* 2005:225–31.

454 7. Roth-Rosenberg D, Aharonovich D, Omta AW *et al.* Dynamic macromolecular composition and high
455 exudation rates in Prochlorococcus. *Limnol Oceanogr* 2021;**66**:1759–73.

456 8. Thornton DCO. Dissolved organic matter (DOM) release by phytoplankton in the contemporary and
457 future ocean. *Eur J Phycol* 2014;**49**:20–46.

458 9. Matteson AR, Rowe JM, Ponsero AJ *et al.* High abundances of cyanomyoviruses in marine ecosystems
459 demonstrate ecological relevance. *FEMS Microbiol Ecol* 2013;**84**:223–34.

460 10. Carlson MCG, Ribalet F, Maidanik I *et al.* Viruses affect picocyanobacterial abundance and
461 biogeography in the North Pacific Ocean. *Nat Microbiol* 2022;**7**:570–80.

462 11. Mruwat N, Carlson MCG, Goldin S *et al.* A single-cell polony method reveals low levels of infected
463 Prochlorococcus in oligotrophic waters despite high cyanophage abundances. *ISME J* 2021;**15**:41–54.

464 12. Beckett SJ, Demory D, Coenen AR *et al.* Disentangling top-down drivers of mortality underlying diel
465 population dynamics of Prochlorococcus in the North Pacific Subtropical Gyre. *Nat Commun*
466 2024;**15**:2105.

467 13. Ribalet F, Swalwell J, Clayton S *et al.* Light-driven synchrony of Prochlorococcus growth and
468 mortality in the subtropical Pacific gyre. *Proc Natl Acad Sci* 2015;**112**:7–11.

469 14. Roth-rosenberg D, Aharonovich D, Omta A *et al.* Dynamic macromolecular composition and high

470 exudation rates in Prochlorococcus. *bioRxiv* 2020.

471 15. Casey JR, Boiteau RM, Engqvist MKM *et al.* Basin-scale biogeography of marine phytoplankton
472 reflects cellular-scale optimization of metabolism and physiology. *Sci Adv* 2022;**8**:eabl4930.

473 16. Geider RJ, La Roche J. Redfield revisited: Variability of C:N:P in marine microalgae and its
474 biochemical basis. *Eur J Phycol* 2002;**37**:1–17.

475 17. Liefer JD, Garg A, Fyfe MH *et al.* The macromolecular basis of phytoplankton C:N:P under nitrogen
476 starvation. *Front Microbiol* 2019;**10**:1–16.

477 18. Jover LF, Effler TC, Buchan A *et al.* The elemental composition of virus particles: Implications for
478 marine biogeochemical cycles. *Nat Rev Microbiol* 2014;**12**:519–28.

479 19. Thompson LR, Zeng Q, Kelly L *et al.* Phage auxiliary metabolic genes and the redirection of
480 cyanobacterial host carbon metabolism. *Proc Natl Acad Sci U S A* 2011;**108**:E757-64.

481 20. Ankrah NYD, May AL, Middleton JL *et al.* Phage infection of an environmentally relevant marine
482 bacterium alters host metabolism and lysate composition. *ISME J* 2014;**8**:1089–100.

483 21. Chevallereau A, Blasdel BG, De Smet J *et al.* Next-Generation "-omics" Approaches Reveal a
484 Massive Alteration of Host RNA Metabolism during Bacteriophage Infection of Pseudomonas
485 aeruginosa. *PLoS Genet* 2016;**12**:1–20.

486 22. Xiao X, Guo W, Li X *et al.* Viral Lysis Alters the Optical Properties and Biological Availability of
487 Dissolved Organic Matter Derived from Prochlorococcus Picocyanobacteria. Johnson KN (ed.). *Appl*
488 *Environ Microbiol* 2021;**87**:1–19.

489 23. Fang X, Liu Y, Zhao Y *et al.* Transcriptomic responses of the marine cyanobacterium
490 Prochlorococcus to viral lysis products. *Environ Microbiol* 2019;**21**:2015–28.

491 24. Azam F, Malfatti F. Microbial structuring of marine ecosystems. *Nat Rev Microbiol* 2007;**5**:782–91.

492 25. Biller SJ, Coe A, Roggensack SE *et al.* Heterotroph Interactions Alter Prochlorococcus Transcriptome
493 Dynamics during Extended Periods of Darkness. Mason O (ed.). *mSystems* 2018;**3**:1–18.

494 26. Braakman R, Follows MJ, Chisholm SW. Metabolic evolution and the self-organization of
495 ecosystems. *Proc Natl Acad Sci* 2017;**114**:E3091–100.

496 27. Calfee BC, Glasgo LD, Zinser ER. Prochlorococcus Exudate Stimulates Heterotrophic Bacterial
497 Competition with Rival Phytoplankton for Available Nitrogen. Martiny JBH (ed.). *MBio* 2022;**13**, DOI:
498 10.1128/mbio.02571-21.

499 28. Becker JW, Hogle SL, Rosendo K *et al.* Co-culture and biogeography of Prochlorococcus and
500 SAR11. *ISME J* 2019;**13**:1506–19.

501 29. Kujawinski EB, Braakman R, Longnecker K *et al.* Metabolite diversity among representatives of
502 divergent Prochlorococcus ecotypes. Gilbert JA (ed.). *mSystems* 2023;**8**, DOI: 10.1128/msystems.01261-
503 22.

504 30. Givati S, Forchielli E, Aharonovich D *et al.* Diversity in the utilization of different molecular classes
505 of dissolved organic matter by heterotrophic marine bacteria. Biddle JF (ed.). *Appl Environ Microbiol*
506 2024;**90**:e00256-24.

507 31. Haider MN, Iqbal MM, Nishimura M *et al.* Bacterial response to glucose addition: growth and
508 community structure in seawater microcosms from North Pacific Ocean. *Sci Rep* 2023;**13**:341.

509 32. Eilers H, Pernthaler J, Amann R. Succession of Pelagic Marine Bacteria during Enrichment: a Close
510 Look at Cultivation-Induced Shifts. *Appl Environ Microbiol* 2000;**66**:4634–40.

511 33. Baltar F, Lundin D, Palovaara J *et al.* Prokaryotic Responses to Ammonium and Organic Carbon
512 Reveal Alternative CO2 Fixation Pathways and Importance of Alkaline Phosphatase in the Mesopelagic
513 North Atlantic. *Front Microbiol* 2016;**7**:1–19.

514 34. Weitz JS, Stock CA, Wilhelm SW *et al.* A multitrophic model to quantify the effects of marine

515 viruses on microbial food webs and ecosystem processes. *ISME J* 2015;**9**:1352–64.

516 35. Ma X, Coleman ML, Waldbauer JR. Distinct molecular signatures in dissolved organic matter
517 produced by viral lysis of marine cyanobacteria. *Environ Microbiol* 2018;**20**:3001–11.

518 36. Weinbauer MG, Bonilla-findji O, Chan AMYM *et al.* Synechococcus growth in the ocean may
519 depend on the lysis of heterotrophic bacteria. *J Plankton Res* 2011;**33**:1465–76.

520 37. Pourtois J, Tarnita CE, Bonachela JA. Impact of Lytic Phages on Phosphorus- vs. Nitrogen-Limited
521 Marine Microbes. *Front Microbiol* 2020;**11**, DOI: 10.3389/fmicb.2020.00221.

522 38. Weinbauer MG. Ecology of prokaryotic viruses. *FEMS Microbiol Rev* 2004;**28**:127–81.

523 39. Shelford EJ, Middelboe M, Møller EF *et al.* Virus-driven nitrogen cycling enhances phytoplankton
524 growth. *Aquat Microb Ecol* 2012;**66**:41–6.

525 40. Sterner R., Elser J. *Ecological Stoichiometry: The Biology of Elements from Molecules to the*
526 *Biosphere*., 2002.

527 41. Moreno AR, Martiny AC. Ecological Stoichiometry of Ocean Plankton. *Ann Rev Mar Sci*
528 2018;**10**:43–69.

529 42. Sher D, Segrè D, Follows MJ. Quantitative principles of microbial metabolism shared across scales.
530 *Nat Microbiol* 2024;**9**:1940–53.

531 43. Grossowicz M, Roth-rosenberg D, Aharonovich D *et al.* Prochlorococcus in the lab and in silico : The
532 importance of representing exudation. 2017, DOI: 10.1002/lno.10463.

533 44. Ni T, Zeng Q. Diel Infection of Cyanobacteria by Cyanophages. *Front Mar Sci* 2016;**2**:1–7.

534 45. Blazewicz SJ, Barnard RL, Daly RA *et al.* Evaluating rRNA as an indicator of microbial activity in
535 environmental communities: Limitations and uses. *ISME J* 2013;**7**:2061–8.

536 46. Breitbart M, Thompson LR, Suttle CA *et al.* Exploring the vast diversity of marine viruses.

537 *Oceanography* 2007;**20**:135–9.

538 47. Thompson LR, Zeng Q, Chisholm SW. Gene Expression Patterns during Light and Dark Infection of
539 Prochlorococcus by Cyanophage. Campbell DA (ed.). *PLoS One* 2016;**11**:e0165375.

540 48. Mizuno CM, Guyomar C, Roux S *et al.* Numerous cultivated and uncultivated viruses encode
541 ribosomal proteins. *Nat Commun* 2019;**10**:752.

542 49. Chen L-X, Jaffe AL, Borges AL *et al.* Phage-encoded ribosomal protein S21 expression is linked to
543 late-stage phage replication. *ISME Commun* 2022;**2**:1–10.

544 50. Brüwer JD, Sidhu C, Zhao Y *et al.* Globally occurring pelagiphage infections create ribosome-
545 deprived cells. *Nat Commun* 2024;**15**:3715.

546 51. Laurenceau R, Raho N, Forget M *et al.* Frequency of mispackaging of Prochlorococcus DNA by
547 cyanophage. *ISME J* 2021;**15**:129–40.

548 52. Moran MA, Kujawinski EB, Stubbins A *et al.* Deciphering ocean carbon in a changing world. *Proc*
549 *Natl Acad Sci U S A* 2016;**113**:3143–51.

550 53. Szul MJ, Dearth SP, Campagna SR *et al.* Carbon Fate and Flux in Prochlorococcus under Nitrogen
551 Limitation. Gutierrez M (ed.). *mSystems* 2019;**4**:1–16.

552 54. Eigemann F, Rahav E, Grossart H *et al.* Phytoplankton exudates provide full nutrition to a subset of
553 accompanying heterotrophic bacteria via carbon, nitrogen and phosphorus allocation. *Environ Microbiol*
554 2022;**24**:2467–83.

555 55. Hu W, Zhang H, Lin X *et al.* Characteristics, Biodiversity, and Cultivation Strategy of Low Nucleic
556 Acid Content Bacteria. *Front Microbiol* 2022;**13**, DOI: 10.3389/fmicb.2022.900669.

557 56. Lebaron P, Servais P, Agogue H *et al.* Does the High Nucleic Acid Content of Individual Bacterial
558 Cells Allow Us To Discriminate between Active Cells and Inactive Cells in Aquatic Systems ? *Appl*

Environ Microbiol 2001;**67**:1775–82.

57. Alothman A, López-Sandoval D, Duarte CM *et al.* Bacterioplankton dark CO 2 fixation in oligotrophic waters. *Biogeosciences* 2023;**20**:3613–24.

58. Amano C, Willhelm U, Reinthaler T *et al.* Anaplerotic processes are key contributors to dark carbon xation in the ocean. 2024.

59. Baltar F, Herndl GJ. Ideas and perspectives: Is dark carbon fixation relevant for oceanic primary production estimates? *Biogeosciences* 2019;**16**:3793–9.

60. Braun A, Spona-Friedl M, Avramov M *et al.* Reviews and syntheses: Heterotrophic fixation of inorganic carbon – significant but invisible flux in environmental carbon cycling. *Biogeosciences* 2021;**18**:3689–700.

61. Reich T, Belkin N, Sisma-Ventura G *et al.* Significant dark inorganic carbon fixation in the euphotic zone of an oligotrophic sea. *Limnol Oceanogr* 2024;**69**:1129–42.

62. Spona-Friedl M, Braun A, Huber C *et al.* Substrate-dependent CO2 fixation in heterotrophic bacteria revealed by stable isotope labelling. *FEMS Microbiol Ecol* 2020;**96**:1–13.

63. Eigemann F, Rahav E, Grossart HP *et al.* Phytoplankton Producer Species and Transformation of Released Compounds over Time Define Bacterial Communities following Phytoplankton Dissolved Organic Matter Pulses. *Appl Environ Microbiol* 2023;**89**, DOI: 10.1128/aem.00539-23.

64. Hügler, M., & Sievert SM. Beyond the Calvin Cycle: Autotrophic Carbon Fixation in the Ocean. *Ann Rev Mar Sci* 2011;**3**:261–89.

65. Kranzler CF, Busono DA, Walsh GJ *et al.* Taxonomically distinct diatom viruses differentially impact microbial processing of organic matter. *Sci Adv* 2025;**11**, DOI: 10.1126/sciadv.adq5439.

66. Ofaim S, Sulheim S, Almaas E *et al.* Dynamic Allocation of Carbon Storage and Nutrient-Dependent

581 Exudation in a Revised Genome-Scale Model of Prochlorococcus. *Front Genet* 2021;**12**:1–21.

582 67. Forchielli, E., Sher, D., & Segrè D. Metabolic phenotyping of marine heterotrophs on refactored
583 media reveals diverse metabolic adaptations and lifestyle strategies. *Msystems* 2022;**7**:e00070-22.

584 68. Landa M, Burns AS, Roth SJ *et al.* Bacterial transcriptome remodeling during sequential co-culture
585 with a marine dinoflagellate and diatom. *ISME J* 2017;**11**:2677–90.

586 69. Moreno-Cabezuelo JÁ, Gómez-Baena G, Díez J *et al.* Integrated Proteomic and Metabolomic
587 Analyses Show Differential Effects of Glucose Availability in Marine Synechococcus and
588 Prochlorococcus. Hom EFY (ed.). *Microbiol Spectr* 2023;**11**, DOI: 10.1128/spectrum.03275-22.

589 70. Swingley WD, Sadekar S, Mastrian SD *et al.* The Complete Genome Sequence of Roseobacter
590 denitrificans Reveals a Mixotrophic Rather than Photosynthetic Metabolism. *J Bacteriol* 2007;**189**:683–
591 90.

592 71. Ferrer-González FX, Widner B, Holderman NR *et al.* Resource partitioning of phytoplankton
593 metabolites that support bacterial heterotrophy. *ISME J* 2021;**15**:762–73.

594 72. Kieft B, Li Z, Bryson S *et al.* Phytoplankton exudates and lysates support distinct microbial consortia
595 with specialized metabolic and ecophysiological traits. *Proc Natl Acad Sci* 2021;**118**:1–12.

596 73. Moran MA, Belas R, Schell MA *et al.* Ecological Genomics of Marine Roseobacters. *Appl Environ*
597 *Microbiol* 2007;**73**:4559–69.

598 74. Hameed A, Suchithra KV, Lin S-Y *et al.* Genomic potential for inorganic carbon sequestration and
599 xenobiotic degradation in marine bacterium Youngimonas vesicularis CC-AMW-ET affiliated to family
600 Paracoccaceae. *Antonie Van Leeuwenhoek* 2023;**116**:1247–59.

601 75. Noble R, Fuhrman J. Breakdown and microbial uptake of marine viruses and other lysis products.
602 *Aquat Microb Ecol* 1999;**20**:1–11.

603 76. Mayers KMJ, Kuhlisch C, Basso JTR *et al.* Grazing on Marine Viruses and Its Biogeochemical
604 Implications. Prasad VR (ed.). *MBio* 2023;**14**, DOI: 10.1128/mbio.01921-21.

605 77. Middelboe M, Jørgensen NOG. Viral lysis of bacteria: an important source of dissolved amino acids
606 and cell wall compounds. *J Mar Biol Assoc United Kingdom* 2006;**86**:605–12.

607 78. Dubinsky Z, Berman-Frank I. Uncoupling primary production from population growth in
608 photosynthesizing organisms in aquatic ecosystems. *Aquat Sci* 2001;**63**:4–17.

609 79. Wu Z, Dutkiewicz S, Jahn O *et al.* Modeling Photosynthesis and Exudation in Subtropical Oceans.
610 *Global Biogeochem Cycles* 2021;**35**, DOI: 10.1029/2021GB006941.

611 80. Moore LR, Coe A, Zinser ER *et al.* Culturing the marine cyanobacterium Prochlorococcus. *Limnol*
612 *Oceanogr Methods* 2007;**5**:353–62.

613 81. Sullivan MB, Huang KH, Ignacio-Espinoza JC *et al.* Genomic analysis of oceanic cyanobacterial
614 myoviruses compared with T4-like myoviruses from diverse hosts and environments. *Environ Microbiol*
615 2010;**12**:3035–56.

616 82. Smith PK, Krohn RI, Hermanson GT *et al.* Measurement of protein using bicinchoninic acid. *Anal*
617 *Biochem* 1985;**150**:76–85.

618 83. Chomczynski P, Sacchi N. Single-step method of RNA isolation by acid guanidinium thiocyanate-
619 phenol-chloroform extraction. *Anal Biochem* 1987;**1**:581–5.

620 84. Marmur J. A procedure for the isolation of deoxyribonucleic acid from micro-organisms. *J Mol Biol*
621 1961;**3**:208-IN1.

622 85. Simon M, Azam F. Protein content and protein synthesis rates of planktonic marine bacteria. *Mar*
623 *Ecol Prog Ser* 1989;**51**:201–13.

624 86. Reich T, Ben-Ezra T, Belkin N *et al.* A year in the life of the Eastern Mediterranean: Monthly

625 dynamics of phytoplankton and bacterioplankton in an ultra-oligotrophic sea. *Deep Sea Res Part I*
626 *Oceanogr Res Pap* 2022;**182**:103720.

627 87. Nielsen ES. The Use of Radio-active Carbon (C14) for Measuring Organic Production in the Sea.
628 *ICES J Mar Sci* 1952;**18**:117–40.

629 88. Hazan O, Silverman J, Sisma-Ventura G *et al.* Mesopelagic Prokaryotes Alter Surface Phytoplankton
630 Production during Simulated Deep Mixing Experiments in Eastern Mediterranean Sea Waters. *Front Mar*
631 *Sci* 2018;**5**, DOI: 10.3389/fmars.2018.00001.

632 89. Walters W, Hyde ER, Berg-lyons D *et al.* Transcribed Spacer Marker Gene Primers for Microbial
633 Community Surveys. *mSystems* 2015;**1**:e0009-15.

634 90. Callahan BJ, McMurdie PJ, Rosen MJ *et al.* DADA2: High-resolution sample inference from Illumina
635 amplicon data. *Nat Methods* 2016;**13**:581–3.

636 91. R Development Core Team RFFSC. R: A language and environment for statistical computing. 2011.

637 92. Team R. RStudio: integrated development for R. RStudio, PBC. 2020.

638 93. Quast C, Pruesse E, Yilmaz P *et al.* The SILVA ribosomal RNA gene database project: improved data
639 processing and web-based tools. *Nucleic Acids Res* 2012;**41**:D590–6.

640 94. Andrews S. FastQC: a quality control tool for high throughput sequence data. 2010.

641 95. Bushnell B, Rood J, Singer E. BBMerge – Accurate paired shotgun read merging via overlap. Biggs
642 PJ (ed.). *PLoS One* 2017;**12**:e0185056.

643 96. Li D, Liu C-M, Luo R *et al.* MEGAHIT: an ultra-fast single-node solution for large and complex
644 metagenomics assembly via succinct de Bruijn graph. *Bioinformatics* 2015;**31**:1674–6.

645 97. Hyatt D, Chen G-L, LoCascio PF *et al.* Prodigal: prokaryotic gene recognition and translation
646 initiation site identification. *BMC Bioinformatics* 2010;**11**:119.

647 98. Aramaki T, Blanc-Mathieu R, Endo H *et al.* KofamKOALA: KEGG Ortholog assignment based on
648 profile HMM and adaptive score threshold. Valencia A (ed.). *Bioinformatics* 2020;**36**:2251–2.

649 99. von Meijenfeldt FAB, Arkhipova K, Cambuy DD *et al.* Robust taxonomic classification of uncharted
650 microbial sequences and bins with CAT and BAT. *Genome Biol* 2019;**20**:217.

651 100. Langmead B, Salzberg SL. Fast gapped-read alignment with Bowtie 2. *Nat Methods* 2012;**9**:357–9.

652 101. Korotkevich G, Sukhov V, Budin N *et al.* Fast gene set enrichment analysis. *bioRxiv* 2016, DOI:
653 10.1101/060012.

654 102. Spencer Graves, Hans-Peter Piepho LS with help from SD-R. multcompView: Visualizations of
655 Paired Comparisons. 2019.

656 103. Hadley Wickham, Romain François, Lionel Henry KM and DV. dplyr: A Grammar of Data
657 Manipulation. 2023.

658 104. Wickham, H., Averick, M., Bryan, J., Chang, W., McGowan, L., François, R., Grolemund, G.,
659 Hayes, A., Henry, L., Hester, J., Kuhn, M., Pedersen, T., Miller, E., Bache, S., Müller, K., Ooms, J.,
660 Robinson, D., Seidel, D., Spinu, V., … Yutani, H. Wickham, H., H. Welcome to the tidyverse. *J Open*
661 *Source Softw* 2019;**4**:1686.

662 105. Kassambara A. rstatix: Pipe-Friendly Framework for Basic Statistical Tests. 2023.

663 106. Kassambara A. ggpubr: "ggplot2" Based Publication Ready Plots. 2023.

664 107. Jari Oksanen, Gavin L. Simpson, F. Guillaume Blanchet, Roeland Kindt P, Legendre, Peter R.
665 Minchin, R.B. O'Hara, Peter Solymos MHHS, Eduard Szoecs, Helene Wagner, Matt Barbour, Michael
666 Bedward BB *et al.* vegan: Community Ecology Package. 2022.

667 108. Wickham H. ggplot2: Elegant Graphics for Data Analysis. 2016.

668